Supporting Information for

"Modeling Auger Processes with Non-Adiabatic Molecular Dynamics"

Guoqing Zhou, [†] Gang Lu, [‡] Oleg V. Prezhdo [#,†,*]

[†]*Department of Physics and Astronomy, University of Southern California, Los Angeles, CA 90089, USA*

[‡]*Department of Physics and Astronomy, California State University, Northridge, CA 91330, USA*

[#]*Department of Chemistry, University of Southern California, Los Angeles, CA 90089, USA*

1. Coulomb integral with the PAW methodology

This is a summary of the projector augmented-wave (PAW) method for evaluating the Coulomb integral from Kresse and co-workers.[1] The one-electron wave functions φ_a, or orbitals, are derived from the pseudo-orbitals $\tilde{\varphi}_a$ with following linear transformation:[2]

$$|\varphi_a\rangle = |\tilde{\varphi}_a\rangle + \sum_i (|\phi_i\rangle - |\tilde{\phi}_i\rangle)\langle \tilde{p}_i|\tilde{\varphi}_a\rangle \tag{1}$$

where *a* is band index. $\tilde{\varphi}_a$ are expanded in the reciprocal space using plane waves,

$$\langle \mathbf{r}|\tilde{\varphi}_a\rangle = \frac{1}{\Omega^{1/2}} \sum_{\mathbf{G}} C_{a\mathbf{G}}(\mathbf{r}) e^{i\mathbf{G}\cdot\mathbf{r}} \tag{2}$$

where Ω is the volume of the Qigner-Seitz cell. ϕ_i are the all-electron (AE) partial waves, which are the solutions of the radial Schrödinger equation for a non-spin-polarized reference atom at a specific energy ε_i and for a specific angular momentum l_i:

$$\langle \mathbf{r}|\phi_i\rangle = \frac{1}{|\mathbf{r}-\mathbf{R}_i|} u_i(|\mathbf{r}-\mathbf{R}_i|) Y_i(\mathbf{r}-\mathbf{R}_i) \tag{3}$$

where *Y* are the spherical harmonics which depend on the orientation of $\mathbf{r}-\mathbf{R}_i$. $\tilde{\phi}_i$ are the pseudo-partial waves. They are equivalent to ϕ_i outside the core radius r_c and match continuously onto ϕ_i inside the core radius:

$$\langle \mathbf{r}|\tilde{\phi}_i\rangle = \frac{1}{|\mathbf{r}-\mathbf{R}_i|} \tilde{u}_i(|\mathbf{r}-\mathbf{R}_i|) Y_i(\mathbf{r}-\mathbf{R}_i) \tag{4}$$

* Corresponding author, email prezhdo@usc.edu

$\tilde{p}_i$ are the projector functions and are dual to $\tilde{\phi}_i$: $\langle\tilde{p}_i|\tilde{\phi}_j\rangle = \delta_{ij}$. Based on Eq. (1), the total charge density related to orbitals *a* and *b*, $n_{ab}(\mathbf{r}) = \varphi_a^*(\mathbf{r})\varphi_b(\mathbf{r})$, can be written as:

$$n_{ab}(\mathbf{r}) = \tilde{n}_{ab}(\mathbf{r}) - \tilde{n}^1_{ab}(\mathbf{r}) + n^1_{ab}(\mathbf{r}) \tag{5}$$

The terms on the right side are defined as:

$$\tilde{n}_{ab}(\mathbf{r}) = \langle\tilde{\varphi}_a|\mathbf{r}\rangle\langle\mathbf{r}|\tilde{\varphi}_b\rangle \tag{9}$$

$$\tilde{n}^1_{ab}(\mathbf{r}) = \sum_{i,j}\langle\tilde{\phi}_i|\mathbf{r}\rangle\langle\mathbf{r}|\tilde{\phi}_j\rangle\langle\tilde{\varphi}_a|\tilde{p}_i\rangle\langle\tilde{p}_j|\tilde{\varphi}_b\rangle \tag{10}$$

$$n^1_{ab}(\mathbf{r}) = \sum_{i,j}\langle\phi_i|\mathbf{r}\rangle\langle\mathbf{r}|\phi_j\rangle\langle\tilde{\varphi}_a|\tilde{p}_i\rangle\langle\tilde{p}_j|\tilde{\varphi}_b\rangle \tag{11}$$

As such, the Coulomb integral is evaluated as:

$$\begin{aligned}\langle mn|pq\rangle &= \frac{e^2}{2}\int d\mathbf{r}_1 d\mathbf{r}_2 \varphi_m^*(\mathbf{r}_1)\varphi_n^*(\mathbf{r}_2) r_{12}^{-1}\varphi_p(\mathbf{r}_1)\varphi_q(\mathbf{r}_2) \\ &= \frac{e^2}{2}\int d\boldsymbol{r}_1 d\boldsymbol{r}_2 n_{mp}(\mathbf{r_1}) n_{nq}(\mathbf{r_2}) \mathrm{r}_{12}^{-1}\end{aligned} \tag{12}$$

2. Nonadiabatic coupling

The nonadiabatic coupling (NAC) is defined as

$$d_{ij} = -i\hbar < \Phi_i \left|\frac{\partial}{\partial t}\right| \Phi_j > \tag{13}$$

With the Slater determinant representation $|\Phi_i\rangle = |\varphi_1 \ldots \varphi_N\rangle \equiv \left|\prod_k^N \varphi_{i_k}\right\rangle$, Eq.(13) can be expressed as:

$$\begin{aligned} d_{ij} &= -i\hbar \left\langle \prod_k^N \varphi_{i_k} \left| \frac{\partial}{\partial t} \right| \prod_l^N \varphi_{j_l} \right\rangle \\ &= -i\hbar \left\langle \prod_k^N \varphi_{i_k} \left| \sum_l^N \frac{\partial}{\partial t}\varphi_{j_l} \prod_{m,m\neq l}^N \varphi_{j_m} \right\rangle \right. \\ &= \sum_l^N -i\hbar \left\langle \varphi_{i_l} \left| \frac{\partial}{\partial t}\varphi_{j_l} \right\rangle \langle \prod_{k,k\neq l}^N \varphi_{i_k} \right| \prod_{k,k\neq l}^N \varphi_{j_k} \rangle \\ &= \sum_l^N d_{i_l,j_l} \prod_{k,k\neq l}^N \delta_{i_k,j_k} \end{aligned} \tag{14}$$

where $d_{i_l,j_l} = -i\hbar \left\langle \varphi_{i_l} \left| \frac{\partial}{\partial t}\varphi_{j_l} \right\rangle \right.$ is the NAC between orbitals φ_{i_l} and φ_{j_l}. Based on Eq. (14), the NAC are non-zero only for pairs of configurations that differ by no more than one orbital.

3. Time-dependent Kohn-Sham equations and nonadiabatic molecular dynamics

An explicit consideration of a Slater determinant basis is not needed for solving time-dependent (TD) Kohn-Sham (KS) equations. They can be solved numerically on a grid in the position or momentum space.[3, 4] KS orbitals are used in the TDKS theory as an auxiliary construct to make sure that the electron density, which is the key quantity of DFT, corresponds to a wavefunction, and to construct the kinetic energy and other orbital dependent functionals. Adiabatic KS orbitals provide an alternative to the grid representation for solving the TDKS equations. The adiabatic KS representation allows a great reduction of dimensionality, since a small set of relevant adiabatic KS orbitals can be selected by energy.[5-8] The KS representation of the TDKS equations shifts the computational cost to solving the time-independent density functional theory (DFT) problem. The main challenge resides in computing the NAC matrix elements, which can diverge at trivial energy crossings.[9, 10]

A grid representation of the TDKS equations allows one to couple quantum mechanical electrons to classical nuclei in a mean-field manner, leading to the quantum-classical Ehrenfest approximation.[3, 11] The advantages and limitations of the Ehrenfest approximation are well documented.[12-14] In particular, the Ehrenfest approach works well for short-time dynamics. Simulating long-time dynamics of charge carriers in nanoscale systems requires inclusion of detailed balance between transitions upward and downward in energy. Detailed balance is needed for proper description of energy relaxation that leads to thermal equilibrium. Phonon-induced decoherence in the electronic subsystem should be included as well, since it can strongly influence transition times. Incorporation of the detailed balance and decoherence effects requires a choice of a basis, which is provided in our multi-particle simulations by the Slater determinants. While these effects can be incorporated into the Ehrenfest method,[13, 14] we focus on the surface hopping framework, which is commonly used for simulating NAMD.

4. Simulation details

10 Å of vacuum is added along each direction to remove spurious interactions between QD images under periodical boundary conditions. Only the Γ-point is used, because QD is a finite system. After heating and equilibrating the system at 300 K for 5 ps, a 2 ps MD trajectory is generated with a 1 fs timestep using the microcanonical ensemble. The NAC and Coulomb couplings are computed along the trajectory. The 2 ps trajectory is sufficient for simulating the

Auger process, which occurs on a sub-picosecond timescale. For comparison, we performed simulations with just the NAC, turning off the Coulomb interaction. In such case, the electron energy can only be transferred to phonons, and the dynamics involving transition across a large energy gap are slow. We also simulated intraband electron and hole relaxation, and electron-hole recombination. In the absence of a third charge carrier, the nonradiative recombination is slow and occurs by transfer of electronic energy to phonons. In order to simulate the slower processes, we replicated the 2 ps Hamiltonian multiple times under the classical path approximation. [15, 16]

5. Comparison of the Coulomb and nonadiabatic coupling matrix elements

Further insights into the mechanism of the Auger process and electron-hole relaxation are provided by Fig. S1 and Table S1, which report the NAC values d_{ij} and the Coulomb matrix elements V_{ij}. Fig. S1 shows the NAC values between orbitals that may get populated in the NAMD simulation. Notably, the NACs between the HOMO, 1Se, and 1Pe are 1-2 orders of magnitude smaller than the NAC between states in the dense manifolds of the valence and conduction bands. The NAC for adjacent states is around 20 meV in the VB, and around 10 meV in the CB, rationalizing the fast hot-hole relaxation, and a slower hot electron relaxation, Fig. S4 and S5. The NACs between the valence and conduction band edges are 100-fold smaller, less than 0.1 meV, as shown in Table S1 for the NAC between the ground state Φ_0 and excited states $\Phi_{\mathrm{H}}^{\mathrm{L}}$ and $\Phi_{\mathrm{H}}^{\mathrm{L1}}$. This is usually the case for wide gap systems and results in slow charge recombination. Here, the CdSe QD has a gap of 1.4 eV between HOMO and LUMO, and 0.43 eV between LUMO and LUMO+1. The NAC between $1S_{\mathrm{e}}$ and $1P_{\mathrm{e}}$, i.e. between $\Phi_{\mathrm{H}}^{\mathrm{L}}$ and $\Phi_{\mathrm{H}}^{\mathrm{L1}}$, is around 1 meV, much smaller than the value for the intra-band states. This weak phonon-electron scattering leads to the phonon-bottleneck that is expected to slow down the hot electron relaxation, and enhance its lifetime and the optoelectronic performance of QDs. However, the Coulomb matrix elements responsible for the electron-hole interactions are quite large, 20-40 meV between $\Phi_{\mathrm{H}}^{\mathrm{L1}}$ and $\Phi_{\mathrm{Hn}}^{\mathrm{L}}$ (n=1, …, 14), Table S1. The Coulomb coupling provides an additional fast channel for the hot electron relaxation. The Coulomb matrix elements are on the same order or even larger than the NAC in the VB, rationalizing why the Auger process, Fig. 2(a),(b), is faster the intraband hole relaxation, Figs. S4, S5.

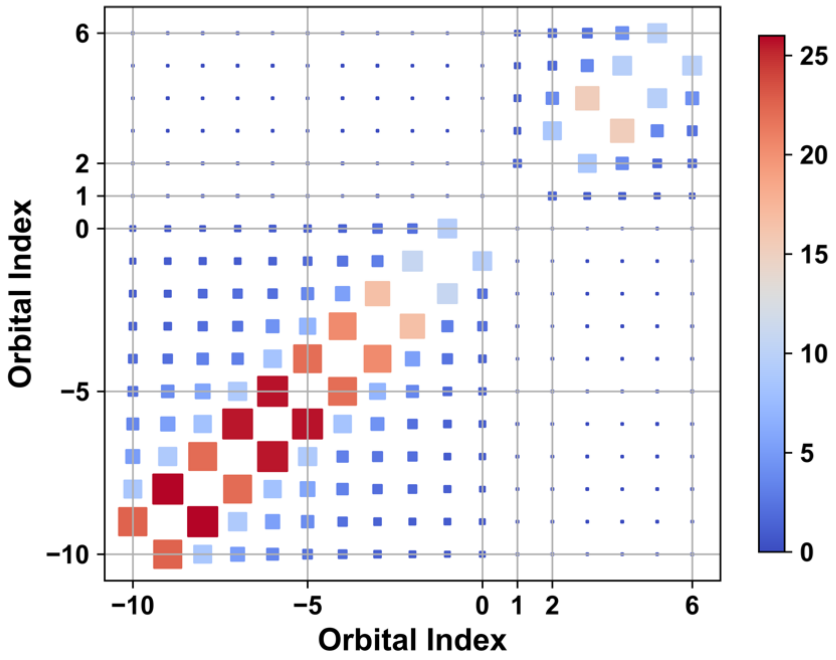

Figure S1. NAC between valence and conduction band orbitals. The orbital index is 0 for HOMO, -5 for HOMO-5, 1 for LUMO, 2 for LUMO+1, etc. The color and size of the squares show the magnitude of NAC between the corresponding orbitals.

State I	**State J**	**Coulomb V_{ij} (meV)**
Φ_{H}^{L1}	Φ_{H1}^{L}	40 ± 30
Φ_{H}^{L1}	Φ_{H14}^{L}~Φ_{H2}^{L}	(10~20) ± (10~20)
State I	**State J**	**NAC d_{ij} (meV)**
Φ_0	Φ_{H}^{L}	0.08 ± 0.06
Φ_{H}^{L}	Φ_{H}^{L1}	1.5 ± 1.4
Φ_0	Φ_{H}^{L1}	0.06 ± 0.04

Table S1. Canonically averaged Coulomb matrix elements and absolute values of NAC matrix elements between selected states. Φ_0 is the ground state, Φ_{Hp}^{Lq} is the excitation from HOMO-p to LUMO+q.

6. Energy flow between electronic and vibrational subsystems in the CdSe quantum dot

Fig. S2 shows decay of the total electronic energy with and without the Coulomb scattering starting from the HOMO → LUMO+1 initial excitation. The electronic energy decay exhibits a fast initial component with the Coulomb interaction turned on, Fig. S2(a). The electron exchanges energy with the hole, and the hole rapidly deposits the energy into phonons. Subsequently, a slow charge recombination follows. The Auger-assisted decay of the electron from $1P_e$ to $1S_e$ occurs on a 0.15 ps timescale. The electron-hole energy exchange is fast because of the strong quantum confinement in the studied small QD. The Auger energy exchange is slower in larger QDs.[17] The energy transferred to the hole relaxes into phonons within 0.2-0.3 ps. Supported further by the charge-phonon relaxation data shown in Figs. S4 and S5, this timescale is typical of intraband charge-phonon relaxation in nanoscale materials.[18-20] The simulation without the Coulomb coupling does not exhibit the fast initial energy decay, Fig. S2(b). Instead, the $1P_e \rightarrow 1S_e$ transition of the electron requires 210 ps, representing the phonon bottleneck, characteristic of decoupled electron and hole.[21, 22] The electron-hole recombination occurs on a nanosecond timescale by coupling to phonons. An Auger-assisted electron-hole recombination requires another charge carrier that can accommodate the energy released during the recombination. This process in not considered in the present simulation.

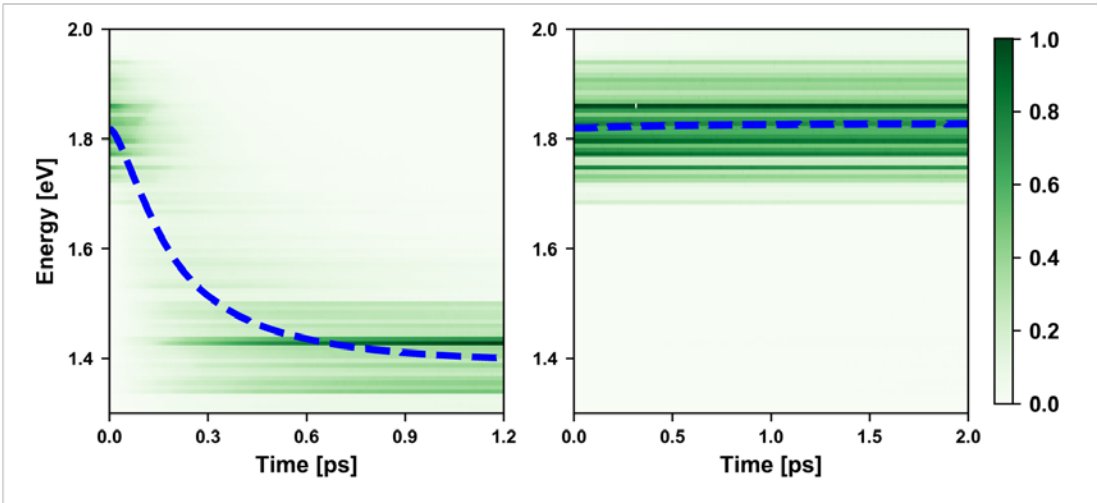

Figure S2. Decay of the total electronic energy starting from the HOMO → LUMO+1 excitation **(a)** with and **(b)** without Coulomb scattering. The color strip shows the energy distribution during the NAMD simulation, and the dashed blue line shows the average energy. The ground state is used as the energy reference.

Further insights into the Auger process are provided in Fig. S3 that shows the evolution of the electron and hole energies, part (a), and the phonon influence spectrum for the intraband hole relaxation, part (b). In the first 0.1 ps, most of the energy lost by the hot electron is transferred to the hole, Fig. S3(a). However, a small fraction of the energy, several tens of meV, is already taken out of the electronic system, because the hot hole immediately starts transferring the energy to phonons. In general, the Auger and phonon driven processes proceed on similar timescales and compete with each other.[23-25] The maximum energy reached by the hot hole is less than 1/3 of the energy released by the electron. The phonon influence spectrum shown in Fig. S3(b) indicates that the hole relaxes by coupling to optical phonons in the 20-40 meV frequency range (150-300 cm^{-1}). The spectrum is computed by Fourier transforming the phonon-induced fluctuations of the energy gaps between HOMO and HOMO-n, where n=1…14, and averaging these fourteen Fourier transforms.

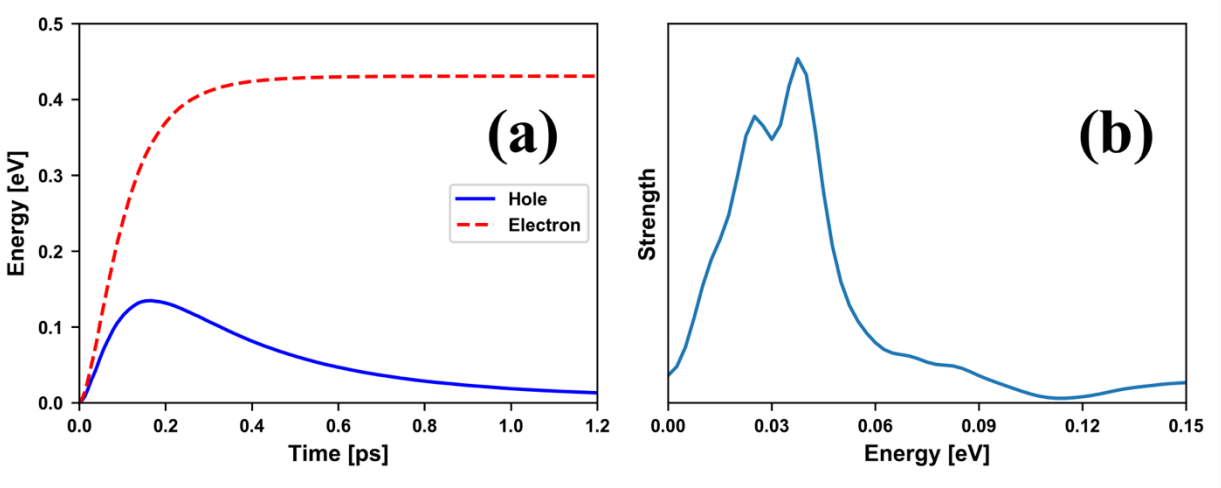

Figure S3. **(a)** Energy transfer from hot electron to hole during the Auger process. The red dashed curve shows the energy lost by the electron. The blue line shows the energy of the hole, which gains energy from the electron and then loses it to phonons. **(b)** Phonon influence spectrum for hot hole relaxation, averaged over transitions between Φ_{H}^{L1} and Φ_{Hn}^{L}: (HOMO-n → HOMO, n=14, 13, …, 1).

In the CdSe QD, the conduction band above the $1P_e$ state and the valence band near the band edge have dense energy spectra, and electron-phonon scattering dominates the carrier relaxation. Therefore, fewest switch surface hopping (FSSH) implemented in PYXAID is used to model hot electron and hole relaxation in these energy ranges.[26, 27] Fig. S4 shows the decay of the

energy of hot electrons initially excited above $1P_e$. The curves are fitted with the exponential function Aexp(-t/τ), where τ is the timescale parameter from fitting. The hot electron relaxation to the edge state $1P_e$ (LUMO+1) shows an average timescale of around 0.3 ps. Fig. S5 presents the decay of the energy of hot holes excited below HOMO. The hole relaxation timescale is within the 0.2~0.3 ps range.

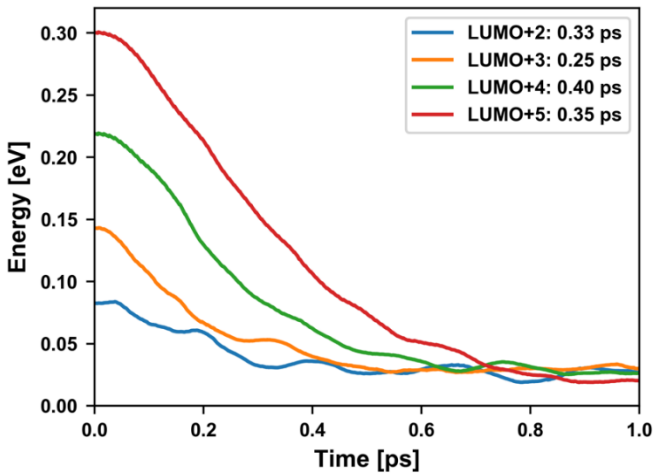

Figure S4. Energy decay of electrons from states LUMO+(2,3,4,5) to $1P_e$ (LUMO+1). The reference zero energy is the energy of LUMO. The timescales are obtained by exponential fits.

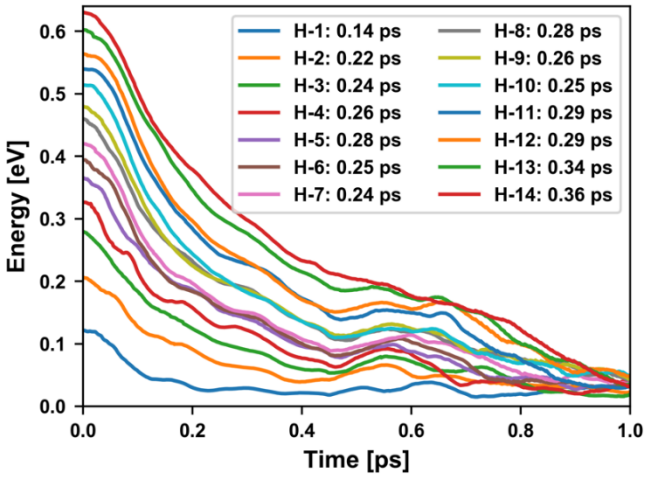

Figure S5. Energy decay of holes from states HOMO-(1, 2,…,14) to HOMO. The reference zero energy is the energy of HOMO. The timescales are obtained by exponential fits.

References:

(1) Paier, J.; Hirschl, R.; Marsman, M.; Kresse, G., The Perdew–Burke–Ernzerhof Exchange-Correlation Functional Applied to the G2-1 Test Set Using a Plane-Wave Basis Set. *Journal of Chemical Physics* **2005**, *122*, 234102.

(2) Blöchl, P. E., Projector Augmented-Wave Method. *Physical Review B* **1994**, *50*, 17953-17979.

(3) Marques, M. A. L.; Castro, A.; Bertsch, G. F.; Rubio, A., Octopus: A First-Principles Tool for Excited Electron-Ion Dynamics. *Computer Physics Communications* **2003**, *151*, 60-78.

(4) Tancogne-Dejean, N.; Oliveira, M. J. T.; Andrade, X.; Appel, H.; Borca, C. H.; Le Breton, G.; Buchholz, F.; Castro, A.; Corni, S.; Correa, A. A., et al., Octopus, a Computational Framework for Exploring Light-Driven Phenomena and Quantum Dynamics in Extended and Finite Systems. *Journal of Chemical Physics* **2020**, *152*, 124119.

(5) Li, L. Q.; Lin, M. F.; Zhang, X.; Britz, A.; Krishnamoorthy, A.; Ma, R. R.; Kalia, R. K.; Nakano, A.; Vashishta, P.; Ajayan, P., et al., Phonon-Suppressed Auger Scattering of Charge Carriers in Defective Two-Dimensional Transition Metal Dichalcogenides. *Nano Letters* **2019**, *19*, 6078-6086.

(6) Trivedi, D. J.; Wang, L.; Prezhdo, O. V., Auger-Mediated Electron Relaxation Is Robust to Deep Hole Traps: Time-Domain Ab Initio Study of Cdse Quantum Dots. *Nano letters* **2015**, *15*, 2086-2091.

(7) Dong, S.; Pal, S.; Lian, J.; Chan, Y.; Prezhdo, O. V.; Loh, Z.-H., Sub-Picosecond Auger-Mediated Hole-Trapping Dynamics in Colloidal Cdse/Cds Core/Shell Nanoplatelets. *ACS Nano* **2016**, *10*, 9370-9378.

(8) Pal, S.; Casanova, D.; Prezhdo, O. V., Effect of Aspect Ratio on Multiparticle Auger Recombination in Single-Walled Carbon Nanotubes: Time Domain Atomistic Simulation. *Nano Letters* **2018**, *18*, 58-63.

(9) Wang, L. J.; Prezhdo, O. V., A Simple Solution to the Trivial Crossing Problem in Surface Hopping. *Journal of Physical Chemistry Letters* **2014**, *5*, 713-719.

(10) Fernandez-Alberti, S.; Roitberg, A. E.; Nelson, T.; Tretiak, S., Identification of Unavoided Crossings in Nonadiabatic Photoexcited Dynamics Involving Multiple Electronic States in Polyatomic Conjugated Molecules. *Journal of Chemical Physics* **2012**, *137*, 014512.

(11) Li, X. S.; Tully, J. C.; Schlegel, H. B.; Frisch, M. J., Ab Initio Ehrenfest Dynamics. *Journal of Chemical Physics* **2005**, *123*, 084106.

(12) Parandekar, P. V.; Tully, J. C., Mixed Quantum-Classical Equilibrium. *Journal of Chemical Physics* **2005**, *122*, 094102.

(13) Akimov, A. V.; Long, R.; Prezhdo, O. V., Coherence Penalty Functional: A Simple Method for Adding Decoherence in Ehrenfest Dynamics. *Journal of Chemical Physics* **2014**, *140*, 194107.

(14) Nijjar, P.; Jankowska, J.; Prezhdo, O. V., Ehrenfest and Classical Path Dynamics with Decoherence and Detailed Balance. *Journal of Chemical Physics* **2019**, *150*, 204124.

(15) Akimov, A. V.; Prezhdo, O. V., Advanced Capabilities of the Pyxaid Program: Integration Schemes, Decoherenc:E Effects, Multiexcitonic States, and Field-Matter Interaction. *Journal of Chemical Theory and Computation* **2014**, *10*, 789-804.

(16) Akimov, A. V.; Prezhdo, O. V., The Pyxaid Program for Non-Adiabatic Molecular Dynamics in Condensed Matter Systems. *Journal of Chemical Theory and Computation* **2013**, *9*, 4959-4972.

(17) Rabani, E.; Baer, R., Distribution of Multiexciton Generation Rates in Cdse and Inas Nanocrystals. *Nano Letters* **2008**, *8*, 4488-4492.
(18) Kilina, S. V.; Kilin, D. S.; Prezhdo, O. V., Breaking the Phonon Bottleneck in Pbse and Cdse Quantum Dots: Time-Domain Density Functional Theory of Charge Carrier Relaxation. *ACS Nano* **2009**, *3*, 93-99.
(19) Long, R.; Casanova, D.; Fang, W. H.; Prezhdo, O. V., Donor Acceptor Interaction Determines the Mechanism of Photoinduced Electron Injection from Graphene Quantum Dots into Tio2:Pi-Stacking Supersedes Covalent Bonding. *Journal of the American Chemical Society* **2017**, *139*, 2619-2629.
(20) Li, L. Q.; Long, R.; Prezhdo, O. V., Charge Separation and Recombination in Two-Dimensional Mos2/Ws2: Time-Domain Ab Initio Modeling. *Chemistry of Materials* **2017**, *29*, 2466-2473.
(21) Pandey, A.; Guyot-Sionnest, P., Slow Electron Cooling in Colloidal Quantum Dots. *Science* **2008**, *322*, 929-932.
(22) Kilina, S. V.; Neukirch, A. J.; Habenicht, B. F.; Kilin, D. S.; Prezhdo, O. V., Quantum Zeno Effect Rationalizes the Phonon Bottleneck in Semiconductor Quantum Dots. *Physical Review Letters* **2013**, *110*, 180404.
(23) Li, L. Q.; Lin, M. F.; Zhang, X.; Britz, A.; Krishnamoorthy, A.; Ma, R. R.; Kalia, R. K.; Nakano, A.; Vashishta, P.; Ajayan, P., et al., Phonon-Suppressed Auger Scattering of Charge Carriers in Defective Two-Dimensional Transition Metal Dichalcogenides. *Nano Lett.* **2019**, *19*, 6078-6086.
(24) Ben-Shahar, Y.; Philbin, J. P.; Scotognella, F.; Ganzer, L.; Cerullo, G.; Rabani, E.; Banin, U., Charge Carrier Dynamics in Photocatalytic Hybrid Semiconductor-Metal Nanorods: Crossover from Auger Recombination to Charge Transfer. *Nano Letters* **2018**, *18*, 5211-5216.
(25) Hyeon-Deuk, K.; Prezhdo, O. V., Time-Domain Ab Initio Study of Auger and Phonon-Assisted Auger Processes in a Semiconductor Quantum Dot. *Nano Letters* **2011**, *11*, 1845-1850.
(26) Akimov, A. V.; Prezhdo, O. V., The Pyxaid Program for Non-Adiabatic Molecular Dynamics in Condensed Matter Systems. *J. Chem. Theor. Comp.* **2013**, *9*, 4959-4972.
(27) Tully, J. C., Molecular Dynamics with Electronic Transitions. *Journal of Chemical Physics* **1990**, *93*, 1061-1071.